

Structure of flux line lattices with weak disorder at large length scales

Philip Kim, Zhen Yao,* Cristian A. Bolle,† and Charles M. Lieber

Division of Engineering and Applied Sciences, Harvard University, Cambridge, Massachusetts 02138

(Received 15 July 1999)

Dislocation-free decoration images containing up to 80 000 vortices have been obtained on high quality $\text{Bi}_2\text{Sr}_2\text{CaCu}_2\text{O}_{8+x}$ superconducting single crystals. The observed flux line lattices are in the random manifold regime with a roughening exponent of 0.44 for length scales up to 80–100 lattice constants. At larger length scales, the data exhibit nonequilibrium features that persist for different cooling rates and field histories. [S0163-1829(99)50142-2]

Recent studies of high-temperature superconductors have shown richness in the phase diagram due to the presence of weak quenched disorder.¹ Larkin showed that arbitrarily weak disorder destroys the long-range translational order of flux lines (FL's) in a lattice.² It was recently pointed out that the Larkin model, which is based on a small displacement expansion of the disorder potential, cannot be applied to length scales larger than the correlated volume of the impurity potential termed the Larkin regime.^{3–5} Beyond the Larkin regime, the behavior of FL's in the absence of dislocations has been considered using elastic models.^{3–5} First, FL's start to behave collectively as an elastic manifold in a random potential with many metastable states (the random manifold regime).³ In this random manifold regime, the translational order decreases as a stretched exponential, whereas there is a more rapid exponential decay in the Larkin regime. At even larger length scales, when the displacement correlation of FL's become comparable to the lattice spacing, the random manifold regime transits to a quasiordered regime where the translational order decays as a power law.^{4,5}

Experimentally, neutron-diffraction⁶ and local Hall-probe measurements⁷ have shown the existence of an order-disorder phase transition with increased field, although the microscopic details of these phases are not clear. Theoretical progress describing FL's in the presence of weak disorder has been made within elastic theory, which proposes the absence of dislocations at equilibrium.^{5,8,9} To date, however, there has been no experimental work addressing the structure of dislocation-free FL lattices at large length scales. Previous magnetic decoration studies^{10,11} showed that the dislocation density decreases and the translational order increases with increasing magnetic field. However, only relatively short-range translational order could be probed in the previous work due to the finite image size and relatively low applied fields.

In this paper, we report the first large length scale structural studies of FL's with measurements extending up to ~ 300 lattice constants and fields up to 120 G. Real-space images show dislocation-free regions containing up to the order of 10^5 FL's. A very low density of dislocations was also observed, although detailed analysis suggests that the dislocations are not equilibrium features. The translational correlation function and displacement correlator have been calculated from dislocation-free data to examine quantitatively

the decay of order. These results show a stretched exponential decay of the translational order indicating that FL's are in the random manifold regime. The experimentally determined roughening exponent in the random manifold regime agrees well with theoretical predictions.

High quality single crystals of $\text{Bi}_2\text{Sr}_2\text{CaCu}_2\text{O}_{8+x}$ (BSCCO) were grown as described elsewhere.¹² Typically, crystals of $\sim 1 \text{ mm} \times 1 \text{ mm} \times 20 \mu\text{m}$ size were mounted on a copper cold finger and decorated with thermally evaporated iron clusters at 4 K. The samples were cooled down to 4 K using different thermal cycles to test nonequilibrium effects and to achieve as close an equilibrium configuration of FL's as possible within the experimental time scale. The FL structure was imaged after decoration using a scanning electron microscope equipped with a 4096×4096 pixel, 8-bit grayscale image acquisition system. Nonlinearity in the system was eliminated using grating standards. This high-resolution system enabled us to acquire images containing nearly 10^3 FL's. In addition, an iterative Voronoi construction¹³ was used to reduce the positioning inaccuracy to 3% of a lattice constant.

Samples were decorated in fields of 70, 80, and 120 G parallel to the c axis of BSCCO single crystals. In contrast to the previous decoration experiments at lower fields,^{10,11} we find that the dislocations are rare at these fields. The density of dislocations was 1.7×10^{-5} , 1.4×10^{-5} , and 3.1×10^{-5} for 70, 80, and 120 G, respectively, where the total number of vortices is $\sim 240\,000$ for each field. It is thus trivial to find many large $100 \times 100 \mu\text{m}^2$ dislocation-free regions in the decorated samples. The size of the largest dislocation-free image, which was obtained in a field of 70 G, is $152 \times 152 \mu\text{m}^2$ with 78 363 vortices.¹⁴ Although a small number of dislocations are detected in our FL images, this does not imply that they are energetically favorable at equilibrium. On the contrary, we believe that the large dislocation-free areas observed in the images provide a lower bound for the length scale of equilibrium dislocation loops. We discuss this point below after presenting a quantitative analysis of the translational order.

To study quantitatively the FL lattice order, we proceed as follows. First, a perfect lattice is constructed and registered to the FL positions obtained from an experimental image. The initial lattice vectors used to construct the perfect lattice were obtained from the Fourier transform of the vortex positions. When an image contains a dislocation, the continuum

approximation is used to construct the perfect lattice with the dislocation.¹⁵ Next we minimized the root-mean-square displacement between the underlying perfect lattice and the real FL lattice by varying the position and orientation of the two lattice vectors of the perfect lattice. The displacement vector $\mathbf{u}(\mathbf{r})$ associated with each of the vortices positioned at \mathbf{r} relative to the perfect lattice was then computed. Figure 1 displays a color representation of the displacement field for a typical dislocation-free image and an image containing three dislocations. In Fig. 1(a), the average displacement is $0.22a_0$, where a_0 is the lattice constant. Qualitatively, the map consists of several intermixed domainlike structures, within which the displacement fields are correlated. These uniformly dispersed domainlike structures of the displacement field produce sharp Bragg peaks in Fourier space [see Fig. 3(b) below]. We also believe that $\mathbf{u}(\mathbf{r})$ provides a quick indication of nonequilibrium effects. For example, Fig. 1(b) exhibits large domains of correlated displacements that are sheared relative to each other; that is, the blue-green-blue coded domains. We believe that this larger scale distortion is a manifestation of a nonequilibrium structure that may arise from quenched dynamics of FL's during our field-cooling process (see below).

To compare our data directly with theoretical predictions,⁵ we have calculated the displacement correlator, $B(r)$, and translational correlation function, $C_{\mathbf{G}}(r)$. $B(r)$ and $C_{\mathbf{G}}(r)$ are defined as $\langle [\mathbf{u}(\mathbf{r}) - \mathbf{u}(\mathbf{0})]^2 \rangle / 2$ and $\langle e^{i\mathbf{G}[\mathbf{u}(\mathbf{x}) - \mathbf{u}(\mathbf{0})]} \rangle$, respectively, where $\langle \rangle$ is the average over thermal fluctuations and quenched disorder, and \mathbf{G} is one of the reciprocal lattice vectors. Theoretically,⁵ we expect $B(r)$ will show three distinct behaviors as r increases: $B(r) \sim r$ in the Larkin regime, where $B(r)$ is less than the square of ξ , the in-plane coherence length. As r increases further, FL's are in the random manifold regime where $\xi^2 < B(r) < a_0^2$. In this regime $B(r) \sim r^{2\nu}$ with the roughening exponent $2\nu (< 1)$. Finally, at the largest length scales (the quasicrystalline regime) where $a_0^2 < B(r)$, $B(r) \sim \ln r$. Since the in-plane ξ of BSCCO is only $\sim 20 \text{ \AA}$, the Larkin regime is irrelevant in our experiment (i.e., $a_0 \gg \xi$). Figure 2(a) shows the behavior of $B(r)$ calculated from the data in Fig. 1(a). For $r < 80a_0$, $B(r)$ can be fit well with a power law, $B(r) \sim r^{2\nu}$, with $2\nu = 0.44$. Thus, our experiment is probing the random manifold regime at least up to this scale. Indeed, $B(r)$ grows only up to $0.05 a_0^2$ at $r = 80a_0$, well below the expected crossover to the quasicrystalline regime, i.e., $B(r) \sim a_0^2$. A naive extrapolation to $B(r) = a_0^2$ suggests the crossover at $r \sim 10\,000a_0$ ($\sim 4 \text{ mm}$), which is far beyond our experimental limit. Samples with such a large clean area, and direct imaging of $\sim 10^8$ vortices would be required to observe the logarithmic roughening of FL's. The roughening exponent 2ν is found to be independent of the field (70–120 G) and consistent with the estimate $2\nu = 2/5$ obtained by Feigelman *et al.* using a scalar argument.³ As shown in Fig. 2(b), $C_{\mathbf{G}}(r)$ and $e^{-G^2 B(r)/2}$ overlap with each other for $r < L^*$, where the measured L^* is $\sim 80a_0$. These results support the Gaussian approximation, $C_{\mathbf{G}}(r) \approx e^{-G^2 B(r)/2}$, which has been simply assumed for the equilibrium FL's lattice⁵ within this length scale. For $r > L^*$, however, $B(r)$ deviates strongly from expected behavior; that is, $B(r)$ saturates and even decreases as r increases. In addition, the Gaussian approximation breaks down for r

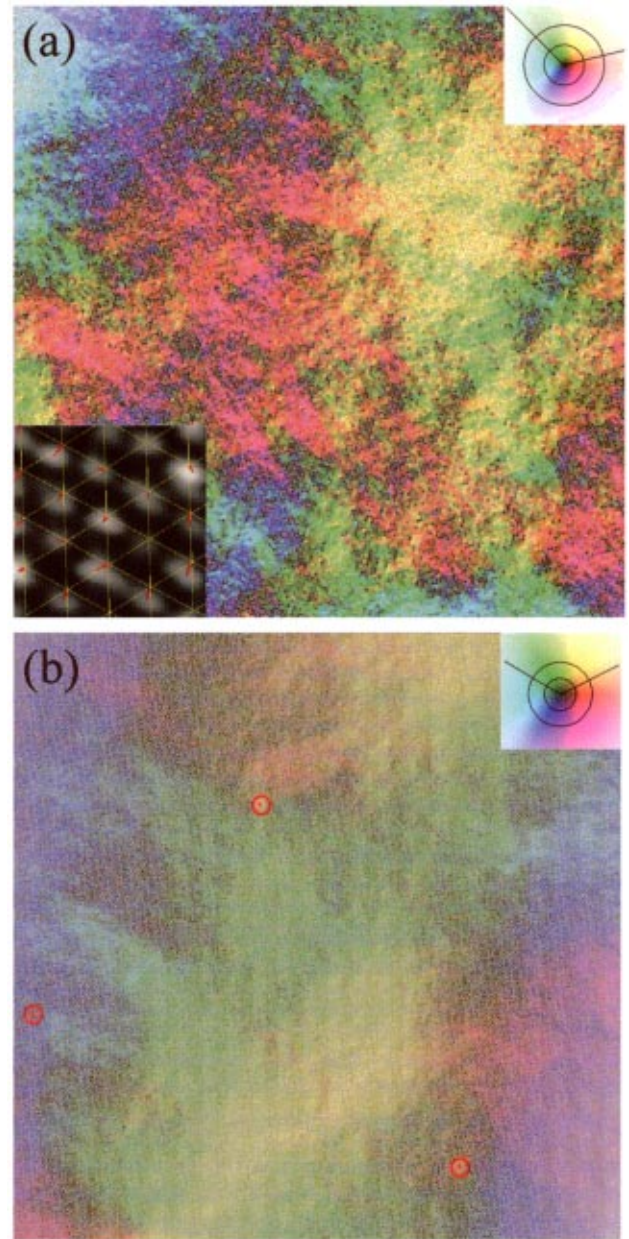


FIG. 1. (Color) Spatial map of vortex displacements $\mathbf{u}(\mathbf{r})$ from the perfect lattice positions. The darker (brighter) regions in the map correspond to smaller (larger) displacements. Different colors correspond to vortex displacements in different directions, as shown in the inset color wheel. The two solid lines, inner, and outer circles in the color wheel correspond to two basis vectors of the lattice, displacements of $0.5a_0$ and a_0 , respectively. The samples were decorated at 70 G. (a) A dislocation-free image containing 37 003 vortices. The edge of the image corresponds to $106 \mu\text{m}$. The lower inset shows a part of both real FL images and a perfect lattice (yellow) with displacement vectors (red). (b) A larger scale image containing three dislocations (highlighted by red dots and circles) and large-scale shearing. The image contains 78 385 vortices in the $160 \times 160 \mu\text{m}^2$ area.

$> L^*$ as evidenced by the difference between $C_{\mathbf{G}}(r)$ and $e^{-G^2 B(r)/2}$. We believe that this behavior can be attributed to nonequilibrium FL structures at the larger length scales of our experiment.

To examine this point further, we decompose $B(r)$ into its

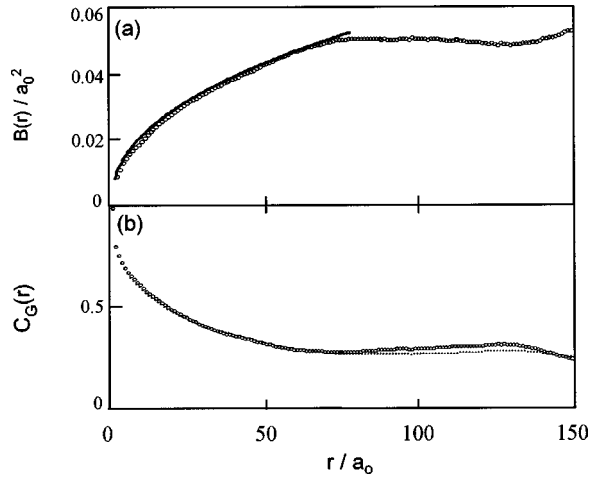


FIG. 2. (a) Mean-square relative displacement correlator $B(r)$ (open circles) as a function of distance \mathbf{r} calculated from the image shown in Fig. 1(a). The solid line is a power-law fit: $B(r) \sim r^{0.44}$. (b) Translational correlation function $C_G(r)$ (dots) calculated from the same image. The open circles are a comparison with the Gaussian approximation: $C_G(r) \approx e^{-G^2 B(r)/2}$.

longitudinal [$B^L(r)$] and transverse [$B^T(r)$] parts: $B(r) = [B^L(r) + B^T(r)]/2$, where

$$B^L(r) = \left\langle \left(\left[\mathbf{u}(r) - \mathbf{u}(0) \right] \cdot \frac{\mathbf{r}}{r} \right)^2 \right\rangle. \quad (1)$$

It is worth noting that in the random manifold regime, the ratio of $B^T(r)$ and $B^L(r)$, is predicted to be $2\nu + 1$,⁵ and thus an independent estimate of the roughening exponent. The average value of this ratio measured from our data [inset to Fig. 3(a)] is 1.40, which is consistent with the value of 2ν obtained from $B(r)$. As shown in Fig. 3(a), both B^L and $B^T(r)$ are described well with the power-law behavior up to $r \sim L^*$. Beyond this range, however, the transverse displacement $B^T(r)$ first deviates from power law causing deviations in $B(r)$. Thus, we infer that shear motion of the FL lattice should be responsible for the abnormal behavior of $B(r)$. Since the shear modulus of FL lattice is much smaller in magnitude than the compressional modulus,¹ $B^T(r)$ is always larger than $B^L(r)$, and the shear motion dominates the relaxation of the FL lattice during the field cooling process. As temperature decreases, the long-wavelength component of shear motion is frozen out. We believe that the domainlike structures seen in Fig. 1 are a snap shot of these frozen long-wavelength shear motions. Note that the characteristic length scale of these domainlike structures in Fig. 1 is again $\sim L^*$, which explains the deviations in $B(r)$ for $r > L^*$. Therefore, L^* is the equilibrium length scale within which FL's can relax to the local equilibrium during our experimental time scale.

This issue can also be addressed through Fourier space analysis. Figure 3(b) displays a blowup of one Bragg peak. Several small satellite peaks appear around the relatively sharp main peak; these satellite peaks indicate a large-scale modulation of the FL lattice. If the FL's were in equilibrium, only one main peak should be expected. The corresponding real-space distance between the main and satellite peaks is, again, $\sim L^*$. Hence, these satellite peaks provide another

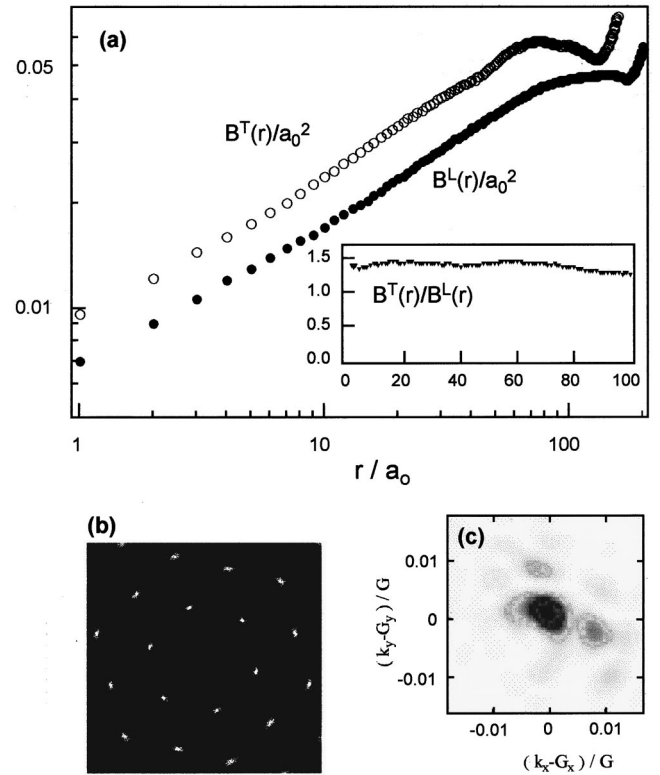


FIG. 3. (a) Transverse (open circle) and longitudinal (solid circle) displacement correlators, i.e., $B^T(r)$ and $B^L(r)$, as a function of distance calculated from Fig. 1(a). The inset shows the ratio of the two quantities. (b) The Fourier space image showing all six first-order Bragg peaks. (c) Detail of one of the Fourier peaks calculated from the same image (inverted gray scale). The dark arrows highlight two satellite peaks.

evidence of the frozen-in dynamics beyond the equilibrium length scale L^* . In addition, we have prepared FL lattices in different ways to address the nonequilibrium structures. For example, we cooled the samples in the absence of a field to 65 K, applied a field 70 G, and then cooled slowly (0.1 K/min) to 4 K. Significantly, we find a similar density of dislocations and FL structure compared to the rapid (10 K/s) field-cooled samples. Since 65 K is far below the melting temperature,¹⁶ this observation suggests that the nonequilibrium structures originate from the frozen-in dynamics far below the melting temperature. Although we can probe FL's up to a length scale of $\sim 300a_0$, there is a much smaller length scale L^* that prohibits direct application of the theory derived for equilibrium FL's. Further studies should address this important issue.

Finally, we consider the origin of dislocations observed in our experiments, since the nonequilibrium vs equilibrium nature of dislocations is critical to the existence of the Bragg glass phase. We believe that our data, which exhibit a small number of dislocations, in fact, favor the nonequilibrium nature of dislocations in the FL lattice for the following reasons. First, it is found that most dislocations are pinned in between domain boundaries [see Fig. 1(b) for example]. If there were a dislocation within the domainlike structures where FL's are locally in equilibrium, the dislocation should be an equilibrium feature.^{13,17} Second, $L^* \ll L_d = n_d^{-1/2} \sim 250a_0$, where L_d and n_d are the average distance between

dislocations and the density of dislocations, respectively. If dislocations were energetically favorable in an equilibrium FL lattice, large dislocation loops should proliferate beyond the equilibrium length scale L^* . In addition, if some dislocations drift within domains, and are pinned at domain boundaries, we should have $L_d \lesssim L^*$. Therefore, our experiment ($L^* \ll L_d$) suggests that dislocations are not equilibrium features in the FL lattice. Together, our data provide a lower bound for the length scale of equilibrium dislocation loops in the FL lattice.

In summary, we have obtained large scale dislocation-free images of the FL lattice in high quality BSCCO supercon-

ductors. Quantitative analyses of the translational order indicate that the system is in equilibrium for length scales up to $\sim 80a_0$, and that FL's are in the random manifold regime with a roughening exponent $2\nu=0.44$. We suggest that the very small density of dislocations observed in our data is an out-of-equilibrium feature due to the short time scales involved in our field-cooled experiments.

We thank D. R. Nelson, D. S. Fisher, P. Le Doussal, and T. Giamarchi for helpful discussions. C.M.L. acknowledges support of this work by the NSF Division of Materials Research.

*Present address: Department of Applied Physics and DIMES, Delft University of Technology, Lorentzweg 1, 2628 CJ Delft, The Netherlands.

[†]Present address: Bell Laboratories, Lucent Technologies, 700 Mountain Avenue, Murray Hill, NJ 07974.

¹G. Blatter, M. V. Feigelman, V. M. Genshkenbein, A. I. Larkin, and V. M. Vinokur, *Rev. Mod. Phys.* **48**, 1125 (1994).

²A. I. Larkin, *Zh. Eksp. Teor. Fiz.* **58**, 1466 (1970) [*Sov. Phys. JETP* **31**, 784 (1970)].

³M. V. Feigelman, V. M. Genshkenbein, A. I. Larkin, and V. M. Vinokur, *Phys. Rev. Lett.* **63**, 2303 (1989).

⁴T. Nattermann, *Phys. Rev. Lett.* **64**, 2454 (1990).

⁵T. Giamarchi and P. Le Doussal, *Phys. Rev. Lett.* **72**, 1530 (1994); *Phys. Rev. B* **52**, 1242 (1995).

⁶R. Cubitt, E. M. Forgan, G. Yang, S. L. Lee, D. Mck. Paul, H. A. Mook, M. Yethiraj, P. H. Kes, T. W. Li, A. Menovsky, Z. Tarnawski, and K. Mortensen, *Nature (London)* **365**, 407 (1993).

⁷B. Khaykovich, E. Zeldov, D. Majer, T. W. Li, P. H. Kes, and M.

Kanczykowski, *Phys. Rev. Lett.* **76**, 2555 (1996).

⁸D. S. Fisher, *Phys. Rev. Lett.* **78**, 1964 (1997).

⁹J. Kierfeld, T. Nattermann, and T. Hwa, *Phys. Rev. B* **55**, 626 (1997).

¹⁰D. G. Grier, C. A. Murray, C. A. Bolle, P. L. Gammel, and D. J. Bishop, *Phys. Rev. Lett.* **66**, 2270 (1991).

¹¹P. Kim, Z. Yao, and C. M. Lieber, *Phys. Rev. Lett.* **77**, 5118 (1996).

¹²Y. Li, J. Liu, and C. M. Lieber, *Phys. Rev. Lett.* **70**, 3494 (1993).

¹³P. Kim, Ph.D. thesis, Harvard University, 1999.

¹⁴Due to the resolution limit of ordinary printed material, we cannot present our raw data, and delaunay triangulations here. They can be found in our web site: <http://magic.harvard.edu/decoration/>

¹⁵P. M. Chaikin and T. C. Lubensky, *Principles of Condensed Matter Physics* (Cambridge University, Cambridge, 1995).

¹⁶D. Majer, E. Zeldov, and M. Konczykowski, *Phys. Rev. Lett.* **75**, 1166 (1996).

¹⁷P. Kim, Z. Yao, C. A. Bolle, and C. M. Lieber (unpublished).